Electronic Supplementary Material (ESI) for Journal of Materials Chemistry A.

Supplementary information

Vanadium nitride encapsulated carbon fibre networks with furrowed porous surfaces for ultrafast asymmetric supercapacitors with robust cycle life

Geon-Hyoung An[a], Do-Young Lee[b], Hyo-Jin Ahn*[ab]

[a]Program of Materials Science & Engineering, Convergence Institute of Biomedical Engineering and Biomaterials, Seoul National University of Science and Technology, Seoul 139-743, Korea

[b]Department of Materials Science and Engineering, Seoul National University of Science and Technology, Seoul 139-743, Korea

1. Experimental section

---

*Corresponding author.

E-mail address: hjahn@seoultech.ac.kr (H.-J. Ahn)

1.1 Chemicals

Vanadyl acetylacetonate ($VO(acac)_2$, 98%), Polyacrylonitrile (PAN, $M_w = 150{,}000$), and *N,N*-Dimethylformamide (DMF, 99.8%) were purchased from Sigma-Aldrich. Vanadium nitride (VN) was purchased from Nanoshel (APS: 80-100nm). All chemicals were used without further purification.

1.2 Synthesis of the walnut-like vanadium nitride encapsulated carbon fibre networks (VN/CF)

The walnut-like vanadium nitride encapsulated carbon fibre networks (VN/CF) were successfully synthesized using electrospinning, the stabilization, and the carbonization. First, $VO(acac)_2$ and PAN were dissolved in DMF. The applied voltage and feed rate were fixed at ~10 kV and 0.05 mL h^{-1}, respectively, during electrospinning process. The as-spun fibre was stabilized for 12 h in air to perform the dehydrogenation of $VO(acac)_2$. The temperature during the stabilization was maintained at 150, 180, and 200 °C to obtain the optimized samples. Finally, the stabilized fibres were carbonized at 800 °C for 2 h in a nitrogen atmosphere. The optimized sample was obtained at 180 °C (referred to as VN/CF).

1.3 Characterization

The structures and morphologies and of the samples were examined by field–emission scanning electron microscopy and transmission electron microscopy (Gwangju Center, Korea Basic Science Institute). The crystal structures and chemical bonding states were investigated using X-ray diffractometry with Cu K_α radiation and X-ray photoelectron spectroscopy with an Al K_α X-ray source, respectively. The surface features such as the specific surface area, average pore diameter, and pore volume were identified by the Brunauer–Emmett–Teller (BET) and Barrett–Joyner–Halenda (BJH) methods using N_2 adsorption. Differential scanning calorimetry (DSC, Shimadzu DSC-60) analyses were carried out to investigate the phase transition change from 50 to 550 °C at a heating rate of 10 °C min^{-1} under a nitrogen atmosphere.

1.4 Electrochemical characterization

Electrochemical measurements were prepared using the conventional three-electrode system composed of a glassy-carbon electrode as a working electrode, a Ag/AgCl reference electrode (saturated KCl), and a platinum wire as a counter electrode. The slurries for the working electrodes, which were made using the prepared sample, ketjen black (KJB, Alfa Aesar), and polyvinylidene difluoride (PVDF, Alfa Aesar) at a ratio of 8:1:1 in N-methyl-2-pyrrolidone (NMP, Samchun). The resultant electrodes were dried in air at 80 °C for 1 h. The electrolyte used was a 1 M KOH solution. The charging/discharging measurements were performed at a current density of 4–80 A g^{-1} in the potential range of –1.2–0.0 V. Cyclic voltammetry (CV) measurements were analysised using a potentiostat/galvanostat (Autolab PGSTAT302N, FRA32M) at a scan rate of 10–200 mV s^{-1}. In addition, the supercapacitors were prepared using the two-electrode system composed of VN/CF as an anode electrode and an $Ni(OH)_2$ as an cathode electrode. The paste was coated on current collector, and dried in air at 100 °C for 12 h. CV measurements were analysised using a potentiostat/galvanostat (Autolab PGSTAT302N, FRA32M) at a scan rate of 10–200 mV s^{-1}. The charging/discharging measurements were performed at a current density of 4–80 A g^{-1} in the potential range of 0.0–1.6 V. The cycling stability of the electrodes was investigated at a current density of 4, 40, and 80 A g^{-1} up to 10,000 cycles. In addition, the specific capacitance of the electrode can be calculated from the discharge curve according to following equation: [1,2,4,5]

$$C_{sp} = I/(mV/dt) \qquad (1)$$

where I (A) is the charging and discharging current, m (g) is the total mass of the active material, V is the voltage drop upon discharging, and dt (s) is the total discharging time.

The energy density (E, Wh kg^{-1}) and power density (P, W kg^{-1}) are calculated based on galvanostatic charging/discharging tests by using the following equation: [1,2,4,5]

$$E = 0.5CV^2 \tag{2}$$

$$P = E/\mathrm{d}t \tag{3}$$

where C is specific capacitance, V is discharging voltage, and dt is the total discharge time.

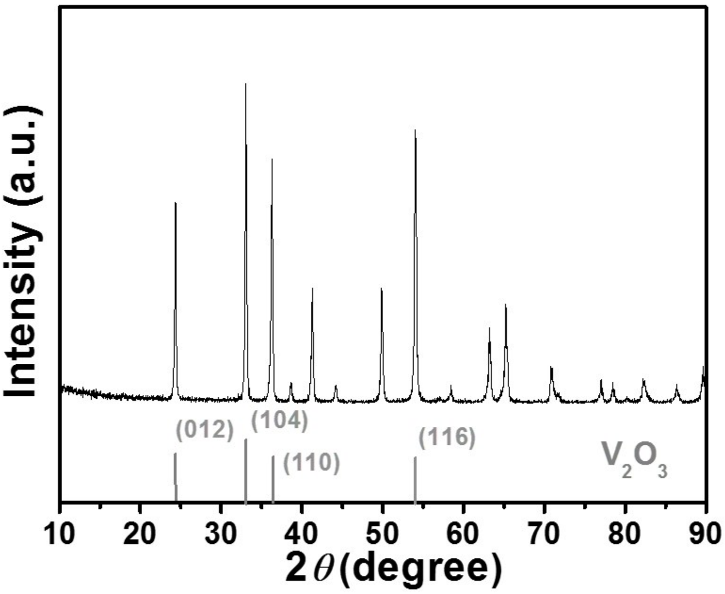

Fig. S1. XRD pattern of carbonized vanadyl acetylacetonate without PAN at 800 °C for 2 h in a nitrogen atmosphere.

Vanadyl acetylacetonate (VO(acac)2, 98%) as precursor without PAN was carbonized at 800 °C for 2 h in a nitrogen atmosphere to confirm the clearer description of the reaction mechanism for the formation of VN. These sample shows diffraction peaks at 24.3°, 33.0°, 36.2°, 41.2°, and 53.9°, corresponding to the (012), (104), (110), (113), and (116) planes of V_2O_3 with a rhombohedral structure. Therefore, the N atoms of VN were originated from PAN during a carbonization process.

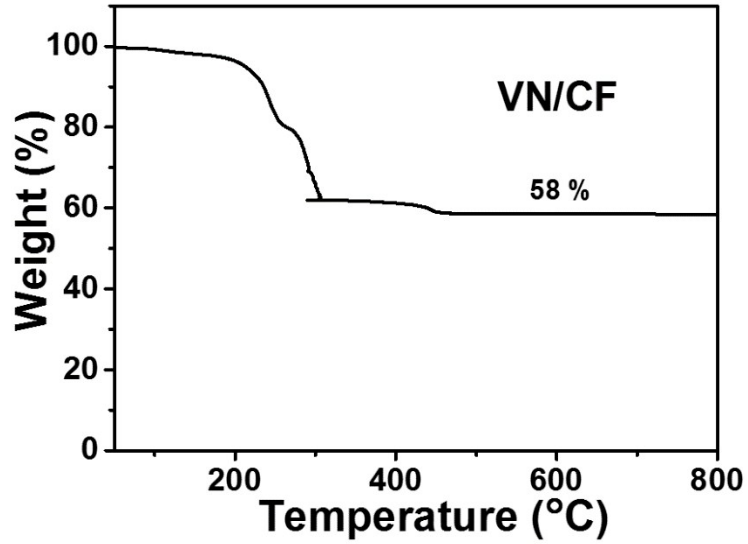

Fig. S2. TGA curve of the VN/CF from 50 to 800 °C at a heating rate of 10 °C min^{-1} in air.

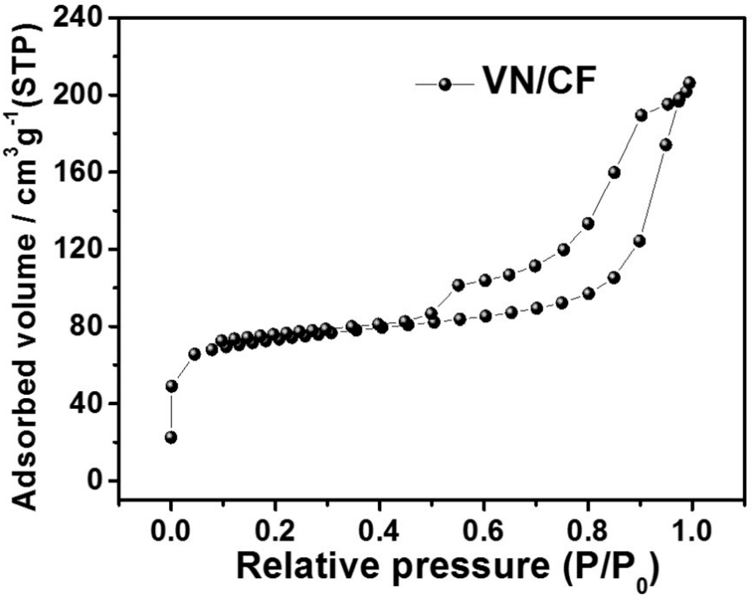

Fig. S3. N_2 adsorption/desorption isotherm of the VN/CF.

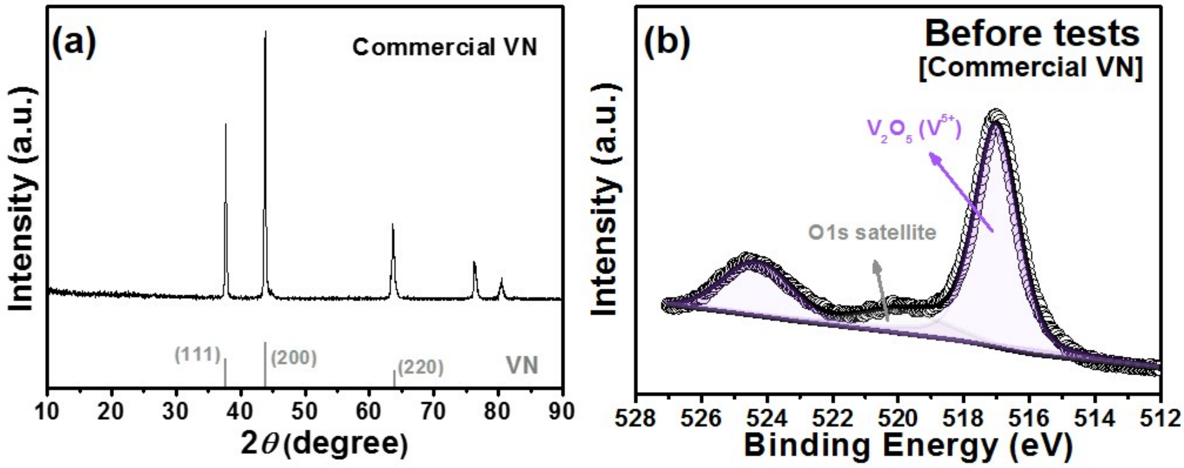

Fig. S4. (a) XRD pattern of a commercial VN. (b) XPS spectra of V 2p for VN/CF.

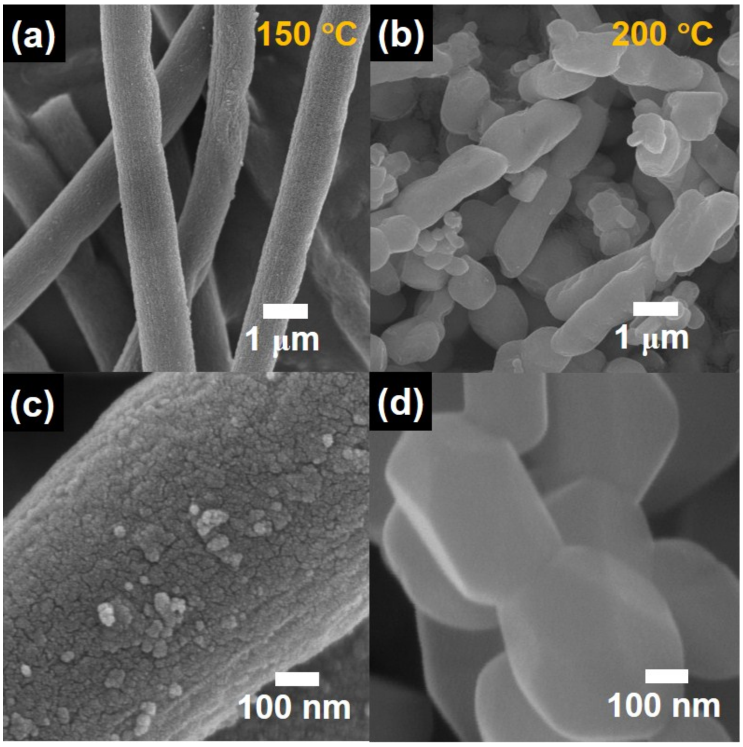

Fig. S5. (a−b) Low-magnification and (c−d) high-magnification SEM images of S-150 and S-200.

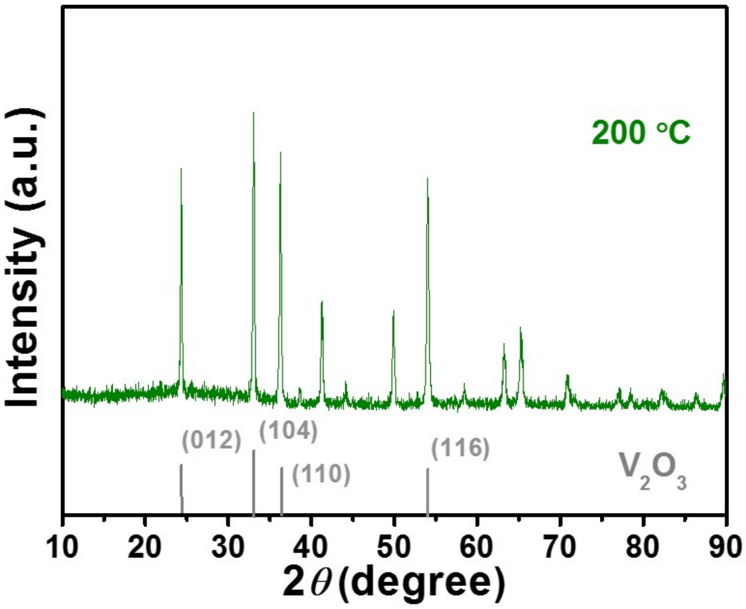

Fig. S6. XRD pattern of S-200.

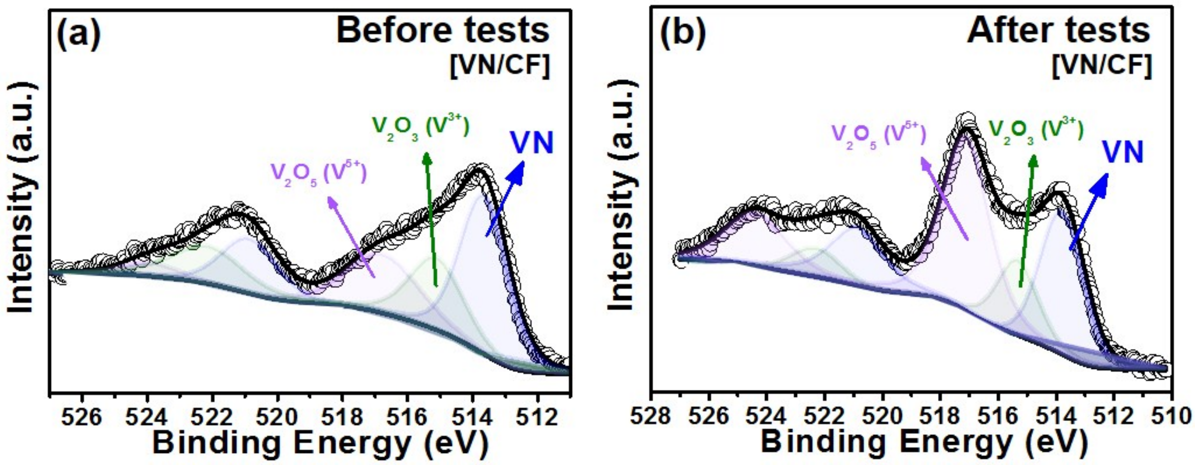

Fig. S7. XPS spectra of V 2p for VN/CF (a) before tests and (b) after tests over the 10,000 cycles.

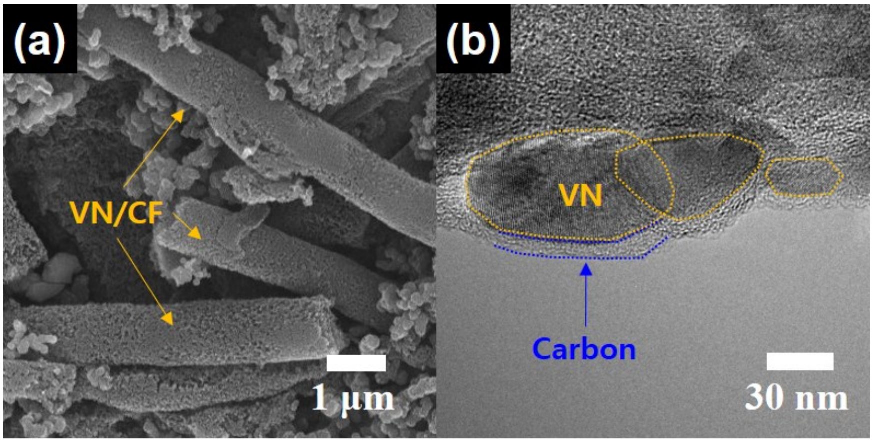

Fig. S8. (a) SEM image and (b) TEM image of VN/CF after the 10,000 cycles.

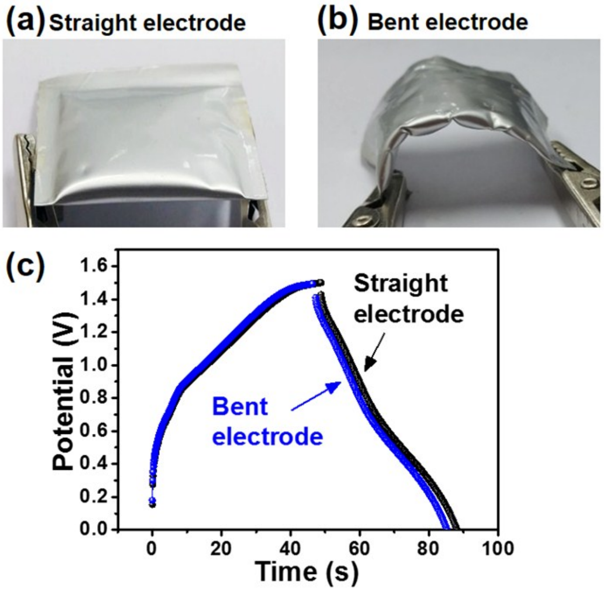

Fig. S9. Preparation of solid-state supercapacitor for VN/CF electrode for bent test using (a) straight and (b) bent electrode. (c) Galvanostatic charge−discharge curves at the current density of 4 A g^{-1} in the potential range of 0.0 to 1.5 V using straight and bent electrodes.

To fabricate the solid-state electrolyte, the 1g polyvinyl alcohol and 1g KOH were mixed in in DI-water at 80 °C for 4 h. In addition, the pouch-type cell was prepared using aluminum laminated film. As shown in Fig. S9, the galvanostatic charge−discharge curves were evaluated at a current density of 4 A g^{-1}. Similar curves are achieved with identical charge–discharge time and redox behaviour even when the electrode was bent by 180°, indicating that the network structure−based VN/CF electrode retains good mechanical stability and shows high flexibility.

Table S1 Energy and power densities compared to previously reported results of asymmetric supercapacitors.

Anode materials	**Cathode materials**	**Energy densities ($Wh\ kg^{-1}$)**	**Power densities ($W\ kg^{-1}$)**	**Ref.**
Activated carbon	$Ni(OH)_2$	21	660	1
VN	$Co(OH)_2$	22−9	160−15,900	2
Activated carbon	$V_2O_5 \cdot 0.6H_2O$	29−20	70−2,000	3
VN/C	$Ni(OH)_2$	31.2	774	4
CMK−3	$NiCo_2O_4$@$CoxNi_{1-x}(OH)_2$	31.2−16.5	396−3960.4	5
Activated carbon	$Ni(OH)_2$	35.7−12.6	490−16,700	6
Activated carbon	Ni–Co binary hydroxides	35.7−19.1	875−7,000	7
Reduced graphene oxide	$NiCo_2S_4$	38.6−28.4	1,330−10,790	8
VN/C	MnO_2/C	38.7−13.3	7.3−316.2	9
Porous carbon nanosheets	Ni–Co–S/C	43.2−28.4	800−22,100	10
VN/C	$Ni(OH)_2$	47.2−29.7	828.7−4231.1	11
Nitrogen−doped graphene	NiO	50−26	740−14,522	12
VN/CF	$Ni(OH)_2$	53.1−36.0	2,700−54,000	This work

References

1 Y.−Z. Su, K. Xiao, N. Li, Z.−Q. Liu and S.−Z. Qiao, *J. Mater. Chem. A*, 2014, **2**, 13845–13853.

2 R. Wang, X. Yan, J. Lang, Z. Zheng and P. Zhang, *J. Mater. Chem. A*, 2014, **2**, 12724–12732.

3 Q. T. Qu, Y. Shi, L. L. Li, W. L. Guo, Y. P. Wu, H. P. Zhang, S. Y. Guan and R. Holze, *Electrochem. Comm.*, 2009, **11**, 1325–1328.

4 Y. Wu and F. Ran, *J. Power Sources*, 2016, **344**, 1−10.

5 K. Xu, R. Zou, W. Li, Q. Liu, X. Liu, L. An and J. Hu, *J. Mater. Chem. A*, 2014, **2**, 10090–10097.

6 H. B. Li, M. H. Yu, F. X. Wang, P. Liu, Y. Liang, J. Xiao, C. X. Wang, Y. X. Tong and G. W. Yang, *Nat. Comm.*, 2013, **4**, 1894.

7 J. Zhang, J.P. Cheng, M. Li, L. Liu, F. Liu and X. B. Zhang, *J. Electroanal. Chem.*, 2015, **743**, 38–45.

8 F. Lu, M. Zhou, W. L, Q. Weng, C. Li, Y. Xue, X. Jiang, X. Zeng, Y. Bando and D. Golberg, *Nano Energy*, 2016, **26**, 313–323.

9 Y. S. I. Zhitomirsky, *J. Power Sources*, 2014, **7**, 235−242.

10 J. Yang, C. Yu, X. Fan, S. Liang, S. Li, H. Huang, Z. Ling, C. Hao and J. Qiu, *Energy Environ. Sci.*, 2016, **9**, 1299−1307.

11 Y. Yang, L. Zhao, K. Shen, Y. Liu, X. Zhao, Y. Wu, Y. Wang and F. Ran, *J. Power Sources*, 2016, **333**, 61−71.

12 S. Y. Kim, H. M. Jeong, J. H. Kwon, I. W. Ock, W. H. Suh, G. D. Stucky and J. K. Kang, *Energy Environ. Sci.*, 2015, **8**, 188–194.